

# Evolution of the Dark Matter Distribution with 3-D Weak Lensing

D. J. Bacon<sup>1\*</sup>, A. N. Taylor<sup>1</sup>, M. L. Brown<sup>1</sup>, M. E. Gray<sup>2</sup>, C. Wolf<sup>3</sup>,  
K. Meisenheimer<sup>4</sup>, S. Dye<sup>5</sup>, L. Wisotzki<sup>6</sup>, A. Borch<sup>4</sup>, M. Kleinheinrich<sup>4</sup>

<sup>1</sup>*Institute for Astronomy, Royal Observatory Edinburgh, Blackford Hill, Edinburgh, EH9 3HJ, U. K.*

<sup>2</sup>*School of Physics and Astronomy, The University of Nottingham, University Park, Nottingham, NG7 2RD, U.K.*

<sup>3</sup>*Department of Physics, University of Oxford, Keble Road, Oxford OX1 3RH, U.K.*

<sup>4</sup>*Max-Planck-Institut für Astronomie, Königstuhl 17, D-69117, Heidelberg, Germany*

<sup>5</sup>*Astrophysics Group, Blackett Laboratory, Imperial College, Prince Consort Road, London SW7 2BW, U.K.*

<sup>6</sup>*Astrophysikalisches Institut Potsdam, An der Sternwarte 16, D-14482 Potsdam, Germany*

\*email: [djb@roe.ac.uk](mailto:djb@roe.ac.uk)

## ABSTRACT

We present a direct detection of the growth of large-scale structure, using weak gravitational lensing and photometric redshift data from the COMBO-17 survey. We use deep  $R$ -band imaging of two  $0.5 \times 0.5$  square degree fields, affording shear estimates for over 52000 galaxies; we combine these with photometric redshift estimates from our 17 band survey, in order to obtain a 3-D shear field. We find theoretical models for evolving matter power spectra and correlation functions, and fit the corresponding shear correlation functions to the data as a function of redshift. We detect the evolution of the power at the  $7.7\sigma$  level given minimal priors, and measure the rate of evolution for  $0 < z < 1$ . We also fit correlation functions to our 3-D data as a function of cosmological parameters  $\sigma_8$  and  $\Omega_\Lambda$ . We find joint constraints on  $\Omega_\Lambda$  and  $\sigma_8$ , demonstrating an improvement in accuracy by a factor of 2 over that available from 2D weak lensing for the same area.

**Key words:** gravitational lensing—cosmology: cosmological parameters, dark matter, large-scale structure of Universe

## 1 INTRODUCTION

The evolution of the distribution of matter is a topic of central concern to cosmology. We seek to understand the history of matter environments at all epochs, from the near uniform distribution of matter at  $z \simeq 1000$ , to the highly skewed distribution at present. Detailed knowledge of this evolution will lead to precise measurements of cosmological parameters such as the dark energy density  $\Omega_v$ , and its equation of state  $w$  (e.g. Refregier et al 2003, Benabed & van Waerbeke 2003). Furthermore, a comparison of the evolution of dark matter and baryonic matter will afford a deep understanding of the formation of baryonic structures.

There are several approaches available for studying matter evolution. For example, one can compare the matter power spectrum inferred from the Cosmic Microwave Background with that inferred from low-redshift galaxy surveys (e.g. Percival et al 2002, Spergel et al 2003); or if one is principally interested in baryonic structure evolution, one can survey galaxy counts out to higher redshifts and directly observe evolution in the count power spectra (eg Phleps & Meisenheimer 2003). Here, we will study another approach:

direct measurements of matter power spectrum evolution via weak gravitational lensing combined with photometric redshifts.

Weak gravitational lensing has proved to be a highly useful method of obtaining cosmological information. The weak lensing phenomenon is observed as the slight alignment of neighbouring galaxy images, due to light rays being deflected by gravitational potential fluctuations along their light paths. As the deflection is due to the gravitational environment through which the light passes, the phenomenon is sensitive to all matter, both dark and baryonic. Lensing therefore allows measurement of the distribution of the entire matter content of the universe.

The use of weak lensing (often without redshift estimates for individual galaxies) to constrain the matter power spectrum is now well developed. The shear estimates for large numbers of galaxies have been used to measure the statistics of an effective 2-dimensional shear field; theoretical calculations of these statistics can be fit to the data in order to estimate cosmological parameters (see e.g. van Waerbeke et al 2001, Hoekstra et al 2002, Bacon et al 2003,

Brown et al 2003, Jarvis et al 2003) or the statistics can be used to measure the dark matter power spectrum (e.g. Pen et al 2003, who measure the 3-D power spectrum at a fixed redshift).

Now, with the increase in availability of reliable photometric redshifts, there is a great deal of interest in combining redshifts with weak lensing. For example, Wittman et al (2001, 2003) have used shear and redshifts to measure the mass and redshift of two clusters directly from the 3-D shear field. In addition, several recent theoretical studies examine how to directly reconstruct the full 3-D gravitational potential from lensing together with photometric redshifts (Taylor 2001; Hu & Keeton 2003; Bacon & Taylor 2003); this will allow examination of peak statistics to obtain cosmological parameters, and studies of galaxy formation as a function of environment.

A more directly statistical approach to the shear estimators is to use redshifts to permit shear power spectrum tomography (e.g. Seljak 1998, Hu 1999, 2002, Huterer 2002, King & Schneider 2002b, Heavens 2003). In this methodology, the galaxies are divided into several redshift bins, in each of which shear correlation functions or power spectra are measured; by comparing these to theoretical models, cosmological parameters can be estimated. This paper will utilise an extension of this approach. This methodology also forms the starting point for removal of systematic pollutants of the cosmological shear signal such as intrinsic galaxy alignments (Heymans et al 2004, Heymans & Heavens 2003, King & Schneider 2002a,b). An alternative 3-D statistical method (particularly for measuring  $w$  and  $w'$ ) is provided by Jain & Taylor (2003), which is further investigated by Bernstein & Jain (2004).

In this paper, we seek to measure directly the evolution of the matter power spectrum. We will achieve this using a maximum likelihood fit between data and theoretical power spectra evolving with redshift. We will also fit evolving power spectra expected for various values of cosmological parameters, in order to demonstrate the power of this method for precise determinations of dark energy parameters with future large lensing surveys.

We will use the COMBO-17 survey (Wolf et al 2001) to measure the dark matter evolution. This survey has already been extensively studied from a weak shear perspective; in particular, it has yielded precise measurements of mass-to-light correlations for a supercluster (Gray et al 2002), measurements of the shear power spectrum arising from large-scale structure (Brown et al 2003), and 3-D gravitational potential maps (Taylor et al 2004). One of the great assets of the COMBO-17 survey is the existence of accurate photometric redshifts ( $\Delta z \simeq 0.05$ ) for galaxies with  $z \lesssim 1$ . Our previous statistical lensing study with COMBO-17 only used these redshifts to obtain median redshifts for lens and source planes; in this study, we will use the redshifts for each individual galaxy to compare each galaxy pair's distortion with what would be expected theoretically for galaxies at these 3-D positions.

The paper is organised as follows. In section 2, we will describe the construction of the theoretical power spectra which we require. In particular, we discuss the modeling of the underlying evolving matter power spectrum; we go on to discuss the shear power spectra expected given this matter power spectrum. This includes not only power spectra for

shear in a redshift shell, but also for cross power spectra for shears at two different redshifts. We also find inversion equations for moving between shear and matter power spectra, and construct phenomenological models to measure evolution of the power spectra.

We proceed in section 3 to describe the COMBO-17 survey, giving details regarding the observations, photometric redshift estimation and weak shear analysis.

Section 4 describes the analysis of the data. We measure the rate of evolution of the matter power spectrum using a simple model. We also find constraints upon the cosmological constant and amplitude of the power spectrum by fitting models with varying values of these parameters to the 3-D shear field data.

Finally, in section 5 we discuss the implications of our results, and discuss the future development of the method on large shear datasets.

## 2 POWER SPECTRA AND CORRELATION FUNCTIONS

In this section we will describe our approach to calculating theoretical models for the matter power spectrum and shear power spectrum for various cosmologies. We will use these models to compare with the data, in order to measure cosmological parameters. We also describe here how we obtain cross-correlation models for shear estimators at different redshifts, and how one can calculate the matter power spectrum from the shear power spectrum and vice versa. Finally, we will present a phenomenological model suited to a direct measurement of the evolution of the power spectrum.

### 2.1 Matter Power Spectrum

We begin by describing the method used for calculating theoretical matter power spectra for different values of cosmological parameters. This will require us to calculate a full non-linear power spectrum, which we will obtain via the intermediate step of calculating the linear power spectrum. First then, we require a model for the linearly evolving power spectrum  $\Delta^2(k)$  in logarithmic increments of co-moving wavenumber  $k$ . In order to achieve this, we use an initially Harrison-Zeldovich power spectrum, evolved with a transfer function  $T$ , growth factor  $g$  described below, and a  $(1+z)^{-2}$  factor as expected for Einstein-de Sitter linear growth of a matter-dominated expansion (c.f. Bardeen et al 1986):

$$\Delta^2(k, z) = Ak^3 T^2(k) k \frac{g^2(z)}{(1+z)^2 g^2(0)}, \quad (1)$$

where  $A$  is a numerical constant which we will normalise presently. The transfer function  $T$  for the Cold Dark Matter scenario is given by (e.g. Bardeen et al 1986; c.f. Efstathiou, Bond & White 1992, Bond & Efstathiou 1984):

$$T_{\text{CDM}}(k) = \frac{\ln(1 + 2.34q)}{2.34q} \times [1 + 3.89q + (16.1q)^2 + (5.46q)^3 + (6.71q)^4]^{-1/4}, \quad (2)$$

with  $q = k/h\Gamma$ . Here,  $h$  is the present-day Hubble constant  $H_0$  divided by  $100 \text{ km s}^{-1} \text{ Mpc}^{-1}$ , and the ‘shape parameter’  $\Gamma$  is defined as (Sugiyama 1995)

$$\Gamma = \Omega_{m,0} h \exp(-\Omega_{B,0}(1 - \sqrt{2h/\Omega_{m,0}})). \quad (3)$$

This equation introduces the present-day density parameters for matter,  $\Omega_{m,0}$ , and baryons,  $\Omega_{B,0}$ . In order to calculate  $\Delta^2$ , we define a growth parameter  $g$  which describes the difference in growth between a particular cosmology and an Einstein-de Sitter cosmology at a given redshift  $z$  (Carroll et al 1992):

$$g(z) = \frac{5}{2} \Omega_m(z) \left[ \Omega_m^{4/7}(z) - \Omega_v(z) + \left(1 + \frac{1}{2} \Omega_m(z)\right) \left(1 + \frac{1}{70} \Omega_v(z)\right) \right]^{-1}. \quad (4)$$

In turn this equation requires the evolution equations for the density parameters of matter,  $\Omega_m$ , and of the vacuum energy,  $\Omega_v$ ,

$$\Omega_m(z) = \frac{\Omega_{m,0}}{a + (1-a)\Omega_{m,0} + (a^3 - a)\Omega_{v,0}} \quad (6)$$

$$\Omega_v(z) = \frac{a^3 \Omega_{v,0}}{a + (1-a)\Omega_{m,0} + (a^3 - a)\Omega_{v,0}}, \quad (7)$$

where the expansion parameter  $a = 1/(1+z)$ . Now we have the equipment for calculating the linear power spectrum, we can progress to estimating the non-linear evolution of the power spectrum, via the formalism of Smith et al (2003).

This method calculates the fully non-linear power using the insights afforded by the Halo Model (e.g. Ma & Fry 2000, Peacock & Smith 2000, Seljak 2000). The power is decomposed into two terms, a quasi-linear term describing the power from the clustering of halos, and a halo term describing power from the clustering of objects within each halo. Each of these terms is calculated by Gaussian filtering the linear power to find a non-linear threshold wavenumber  $k_\sigma$ , spectral index and spectral curvature. These are used to find 11 coefficients which are functions of the calculated spectral properties; the quasi-linear and halo power terms are then found as functions of the linear power and these coefficients, finally resulting in the full power  $\Delta^2$ . Full details of this procedure can be found in Smith et al (2003).

Finally we move from the dimensionless power  $\Delta^2$  to the standard power spectrum  $P$  via

$$P_{NL}(k, z) = 2\pi^2 \Delta_{NL}^2(k, z)/k^3. \quad (8)$$

We normalise the power spectrum at the present epoch by setting a value for the quantity  $\sigma_8$ , measuring the rms fluctuation of density when smoothed by a top-hat filter with radius  $R = 8h^{-1} \text{ Mpc}$ :

$$\sigma_8^2 = \int_0^\infty k^2 dk P(k, 0) \frac{3}{(kR)^3} (\sin(kR) - kR \cos(kR)). \quad (9)$$

Thus, for particular choices of  $\sigma_8, \Omega_{m,0}, \Omega_{v,0}, h, \Omega_b$  and  $\Omega_k$ , we have a model for the evolving non-linear power spectrum at any required redshift.

## 2.2 Shear Power Spectrum

Now that we have a model for the matter power spectrum at any epoch, we can proceed to calculate the 3-D shear power

spectrum and correlation function. It is convenient to obtain these via the effective convergence  $\kappa$ , a measure of the surface mass density, which is given by (following Bartelmann & Schneider 2001, Ch 6 throughout this section):

$$\kappa(\theta) = \frac{3H_0^2 \Omega_m}{2c^2} \int_0^{r_H} dr W(r) f_K(r) \frac{\delta[f_K(r)\theta, r]}{a(r)}. \quad (10)$$

Here,  $\theta$  represents the position on an image,  $\delta$  is the density perturbation field,  $c$  is the speed of light,  $r_H$  is the comoving radial distance to the horizon, and  $r$  is the comoving radial distance to a given mass concentration:

$$r(z) = \frac{c}{H_0} \int_{a(z)}^1 [a\Omega_m(0) + a^2(1 - \Omega_m(0) - \Omega_v(0)) + a^4\Omega_v(0)]^{-1/2} da. \quad (11)$$

In the equation for  $\kappa$  above we also require the radial coordinate distance  $f_K$ ,

$$f_K(r) = \begin{cases} K^{-1/2} \sin(K^{1/2}r) & (K > 0) \\ r & (K = 0) \\ (-K)^{-1/2} \sinh[(-K)^{1/2}r] & (K < 0) \end{cases} \quad (12)$$

with the curvature  $K$  given by

$$K = \left(\frac{H_0}{c}\right)^2 (\Omega_m + \Omega_v - 1). \quad (13)$$

We also require the weighting factor  $W$ ,

$$W(r) = \frac{f_K(r_s - r)}{f_K(r_s)} H(r_s - r), \quad (14)$$

where  $H$  is the Heaviside function and  $r_s$  is the comoving distance to a particular source galaxy.

We can now find the cross-power between convergence at any two redshifts. In order to do this we use Limber’s equation, which can be formulated (e.g. Bartelmann & Schneider 2001) to state that if we have two projections  $p_i, i = 1, 2$  of the density field  $\delta$ , such that

$$p_i(\theta) = \int dr q_i(r) \delta[f_K(r)\theta, r], \quad (15)$$

for some function  $q_i(r)$ , then the cross power spectrum will be

$$P_{12}(\ell) = \int dr \frac{q_1(r)q_2(r)}{f_K^2(r)} P_\delta\left(\frac{\ell}{f_K(r)}, r\right). \quad (16)$$

If we wish to calculate the cross power of  $\kappa$  between two redshifts, then we see by comparing equations (10) and (15) that we do have two projections of the necessary form, with  $q_i$  given by

$$q_i(r) = \frac{3}{2} \frac{H_0^2}{c^2} \Omega_m \frac{f_K(r)f_K(r_i - r)}{f_K(r_i)} \frac{H(r_i - r)}{a(r)}, \quad (17)$$

so we therefore obtain (noting that the two-point statistics of  $\kappa$  and  $\gamma$  agree, e.g. Blandford et al 1991),

$$P_{\gamma 12}(\ell, z_1, z_2) = \frac{9H_0^4 \Omega_m^2}{4c^4} \int_0^{r_1 < r_2} dr \frac{f_K(r_1 - r)}{f_K(r_1)} \frac{f_K(r_2 - r)}{f_K(r_2)} \frac{1}{a^2(r)} P_\delta\left(\frac{\ell}{f_K(r)}, r\right), \quad (18)$$

where  $\ell$  is the angular wavenumber. In the case where we wish to examine the power of the shear at one particular redshift, we can simplify this to

$$P_\gamma(\ell, z_1) = \frac{9H_0^4\Omega_m^2}{4c^4} \int_0^{r_1} dr \frac{f_K^2(r_1-r)}{f_K^2(r_1)a^2(r)} P_\delta\left(\frac{\ell}{f_K(r)}, r\right). \quad (19)$$

We can obtain corresponding cross-correlation functions for shears at two different redshifts  $z_1, z_2$ . We will use three different correlation functions:  $C_1$  represents  $\langle\gamma_1^a\gamma_1^b\rangle$ , where  $\gamma_1^{a,b}$  represents the first shear component of two galaxies, in a coordinate frame where zero position angle lies along the line joining the galaxies (e.g. Bacon et al 2003).  $C_2$  represents  $\langle\gamma_2^a\gamma_2^b\rangle$ , and  $C = C_1 + C_2$ . Given these definitions, the correlation functions are simple transforms of the power:

$$C(\theta, z_1, z_2) = \int_0^\infty \frac{\ell d\ell}{2\pi} P_{\gamma 12}(\ell, z_1, z_2) J_0(\ell\theta), \quad (20)$$

$$C_1(\theta, z_1, z_2) = \int_0^\infty \frac{\ell d\ell}{4\pi} P_{\gamma 12}(\ell, z_1, z_2) [J_0(\ell\theta) + J_4(\ell\theta)], \quad (21)$$

$$C_2(\theta, z_1, z_2) = \int_0^\infty \frac{\ell d\ell}{4\pi} P_{\gamma 12}(\ell, z_1, z_2) [J_0(\ell\theta) - J_4(\ell\theta)]. \quad (22)$$

These are the 3-D shear correlation functions we have been seeking; we will use these functions to compare our data with various evolving cosmological models.

### 2.3 Power Spectrum Inversion

It is convenient to have a simple means of calculating the shear power spectrum from the matter power spectrum; this has been described in the last section. However, it is also useful to have a means of calculating the matter power spectrum given the shear power spectrum; here we outline how this can be achieved for theoretical models. Noisy data are difficult to invert with this procedure; it would be more convenient to fit models to the data and then use the results of this section to invert these models.

In order to show how to invert the shear power spectrum, we start by considering an integral of the form

$$A(r) \equiv \int_0^r dr' B(r', r), \quad (23)$$

where  $B(r', r)$  is a smooth, continuous function. Carrying out a partial differentiation of  $A$  with respect to  $r$ , we find

$$\frac{\partial A(r)}{\partial r} = \int_0^r dr' \frac{\partial B(r, r')}{\partial r} + B(r, r). \quad (24)$$

This result will be used below in order to untangle the matter power spectrum from its integral projection found in calculating the shear. We also require the result

$$\frac{\partial}{\partial r_1} \left( \frac{f_K(r_1-r)}{f_K(r_1)} \right) = \frac{f_K(r)}{f_K^2(r_1)}, \quad (25)$$

which can be easily verified directly from equation (12). Using these two results repeatedly upon the shear power spectrum  $P_\gamma(l, r)$ , we find that we can calculate the matter power spectrum:

$$P_\delta(k, r_1) = \frac{4c^4}{9H_0^4\Omega_m^2} \frac{a^2(r_1)}{2f_K(r_1)} \left( \frac{\partial^2}{\partial r_1^2} + K \right) \left[ f_K^3(r_1) \frac{\partial P_\gamma(f_K(r_1)k, r_1)}{\partial r_1} \right]. \quad (26)$$

Alternatively, we can find a similar means of calculating

the matter power spectrum from the cross power spectrum of shear at two different redshifts:

$$P_\delta(k, r_1) = \frac{4c^4}{9H_0^4\Omega_m^2} \frac{a^2(r_1)f_K(r_2)}{f_K(r_1)f_K(r_2-r_1)} \frac{\partial}{\partial r_1} \left( f_K^2(r_1) \frac{\partial P_{\gamma 12}(f_K(r_1)k, r_1, r_2)}{\partial r_1} \right). \quad (27)$$

These equations therefore permit us to find the matter power spectrum given a model for the shear power spectrum. Note that upon noisy data, the first and second differentials in this equation can lead to unphysical negative power spectra. Thus we reiterate that a better approach is to fit a continuous shear model to the data which can then be inverted with these equations.

### 2.4 Power Spectrum Model for Slope Phenomenology

We conclude this section with a discussion of models for the matter and shear power spectra which allow us to directly examine the redshift evolution of the power spectrum.

Firstly, suppose we have measured the shear cross-correlation function  $C$  between many redshifts, from which we can calculate the shear power spectrum. We will initially restrict ourselves to power within a redshift shell,  $P_\gamma$ ; we will consider  $P_{\gamma 12}$  later. We will attempt to use our formalism with a simple model for the shear power spectrum: a power law in both the angular and redshift directions, i.e.

$$P_\gamma(l, r) = Al^\alpha r^\beta = Ak^\alpha r^{\alpha+\beta}. \quad (28)$$

The correlation function corresponding to this model, calculated from equation (20) is:

$$C(\theta, r) = \frac{A2^{\alpha-1}\alpha\Gamma(\alpha/2)}{\pi\Gamma(-\alpha/2)} \theta^{-2-\alpha} r^\beta. \quad (29)$$

(One should note more generally that, if  $P_\gamma \propto k^\alpha f(r)$ , then  $C \propto \theta^{-2-\alpha} r^{-\alpha} f(r)$ .)

Hence, if we fit a power law to the correlation function in the angular and redshift directions, we can immediately obtain estimates of the corresponding power-law approximation to the shear power spectrum, and an approximation to the underlying matter power spectrum. To achieve the latter, we use the inversion equation (26); we find that the matter power spectrum is given (in a flat universe) by

$$P_\delta(k, r) = \frac{4c^4}{9H_0^4\Omega_m^2} A(\alpha+\beta)(\alpha+\beta+1)(\alpha+\beta+2)k^\alpha a^2(r)r^{\alpha+\beta-1}. \quad (30)$$

This is a very useful formula; if we can adequately fit the shear power spectrum as a power law in the angular and redshift directions, we can instantly infer the corresponding power law matter power spectrum.

We can attempt a similar approach with the cross power spectrum,  $P_{\gamma 12}$ , with a power law model keeping one redshift fixed:

$$P_{\gamma 12}(l, r_1, r_2) = Al^\alpha r_1^\beta = Ak^\alpha r_1^{\alpha+\beta}. \quad (31)$$

However, this is less successful, as we obtain the following form for the matter power spectrum:

$$P_\delta(k, r_1) = \frac{4c^4}{9H_0^4\Omega_m^2} A(\alpha+\beta)(\alpha+\beta+1)r_2k^\alpha \frac{a^2(r_1)r_1^{\alpha+\beta-1}}{r_2-r_1}. \quad (32)$$

This model fails to be physical; besides an unsightly divergence at  $r_2 = r_1$ , we find that the matter power at the present epoch is either zero or infinite, depending on the power law slope. We therefore conclude that a power law model for the cross shear power is unsuitable for directly calculating the matter power spectrum. Equivalently, we should note that the underlying matter power spectrum which produces a power-law cross shear power spectrum is unphysical.

In order to find a measure of matter power spectrum evolution, able to take into account all the information from the shear cross power spectrum, one can take an alternative approach. We will assume a very simple form for the underlying matter power spectrum,

$$P_\delta(k, r_1) = \frac{4c^4}{9H_0^4\Omega_m^2} Ak^\alpha e^{-sz}, \quad (33)$$

and will restrict ourselves to an underlying  $\Lambda$ CDM geometry in moving from this matter power to the shear predictions. This allows us to directly examine the matter evolution, rather than examining both matter and geometry change. The form chosen for  $P_\delta$  has the advantage of being positive definite as required for power; it is also a good fit to  $\Lambda$ CDM evolution in the non-linear regime that we wish to study.

In order to remove some of the freedom from the above equation, we note that  $\alpha = -1.2$  provides an excellent fit to the angular dependence of the  $\Lambda$ CDM shear correlation function throughout  $z < 1$  and  $1' < \theta < 30'$ . We therefore allow only the matter amplitude  $A$  and redshift evolution slope  $s$  to vary. We will fit the corresponding shear correlation function calculated from equation (18) to the data, allowing us to directly measure the rate of evolution of the power spectrum.

### 3 DATA

Having developed a suitable formalism for examining the 3-D matter power spectrum, we wish to proceed to measure this directly from the COMBO-17 survey (Wolf et al 2001). This survey currently spans 1 square degree, in four widely separated  $0.5 \times 0.5$  square degree fields. One of the fields contains the A901/2 supercluster, and is therefore deemed highly unrepresentative and inappropriate for inclusion in this study (c.f. the significantly anomalous power spectrum measured for this field in Brown et al 2003). One further field (SGP) does not currently have full redshift information available, so this study focuses upon the two remaining fields, centred upon the Chandra Deep Field South (CDFS) and an area with no previously known mass concentrations (S11), but which in reality contains a cluster at  $z = 0.11$ ; Brown et al (2003) show that this does not produce a high power spectrum estimate in this field.

All fields in the survey were observed at the MPG/ESO 2.2m telescope, La Silla, Chile, with the Wide-Field Imager. This is a  $4 \times 2$  array of  $2048 \times 4096$  pixel CCDs, with pixel scale 0.238 arcseconds (c.f. Gray et al 2002).

The key characteristic of the COMBO-17 data which makes it suitable for our purpose is the existence of an extensive catalogue of accurate photometric redshifts for the galaxies in each field. Each COMBO-17 field was observed

in 5 broad-band filters (*UBVRI*) and 12 medium-band filters running from 350nm to 930nm. This permits simultaneous estimates of redshift and SED classification using empirically-based spectral templates; this is described in detail in Wolf et al (2001), who use the same version of the catalogue. The resulting accuracy of photometric redshift is  $\Delta_z \simeq 0.05$  for galaxies with  $z < 1.0$ .

The weak shear measurements were made upon the  $R$  filter images from the survey. This filter was used in the best seeing conditions, providing a deep image optimal for weak lensing; the combined exposure length was 36120 seconds for the CDFS field, and 18100 seconds for the S11 field.

The reduction process for this  $R$  band imaging data is described in Gray et al (2002) and Brown et al (2003). For the CDFS field,  $78 \times 8$  CCD chip exposures were registered by using linear astrometric fits, including a  $3\sigma$  rejection of bad pixels and columns; for the S11 field,  $44 \times 8$  exposures were registered in this fashion.

The shear estimation for the galaxies was carried out using the *imcat* package, following the methodology of Kaiser, Squires & Broadhurst (1995); see Gray et al (2002) and Brown et al (2003) for details of the implementation for our dataset. The analysis yields a catalogue of galaxies with centroid positions, plus shear estimates which have been corrected for circularisation of the galaxies by the PSF, and anisotropic smearing due to e.g. tracking errors. This catalogue was combined with the photometric redshift catalogue for the COMBO-17 survey.

The resulting catalogue included 52139 galaxies, 23102 of which had reliable photometric redshifts assigned; the remaining galaxies yielded ambiguous redshift probabilities or were fainter than the  $R = 24$  reliability limit for redshifts in the survey. This remainder of galaxies was flagged as having unreliable redshifts; the faint galaxies were assigned an optional redshift which we use below when stated. Following Brown et al (2003), Section 4, we use a median-magnitude median-redshift relation to assign this redshift; the median  $R$  magnitude of the faint sample is  $R = 24.9$ , corresponding to a median redshift  $z \simeq 0.95 \pm 0.05$ .

### 4 ANALYSIS

We will now use the models developed above to assess the evidence for evolution of the matter distribution from the COMBO-17 survey. We begin by making a minimal direct detection of evolution, by comparing the growth of the lensing signal with redshift to that expected with a truly unevolving matter distribution. We go on to use our phenomenological model of an evolving power spectrum to constrain the rate of evolution. Finally, we return to full power spectra models including cosmological parameters, in order to constrain the cosmological constant from the rate of growth of the shear signal with redshift.

#### 4.1 Preliminary detection of evolution

As a preliminary first step in using 3-D shear data to measure evolution, we will demonstrate that the data exclude a non-evolving matter distribution, given the present-day normalisation of the matter power spectrum  $\sigma_{8,0}$  and a  $\Lambda$ CDM geometry. It is important to realise that this simplest step is

already effectively achieved by 2D cosmic shear surveys, if the median redshift of the survey is well estimated. That is to say, the amplitude of the projected 2D shear field correlation functions measured with cosmic shear surveys (see e.g. van Waerbeke & Mellier 2003, Refregier 2003 for reviews) at a median redshift  $z_m \sim 1$  is inconsistent with that expected for an unevolving power spectrum, both calculated for example with  $\sigma_{8,0} = 0.84 \pm 0.04$  (c.f. Spergel et al 2003). For example, at an angular scale of  $1'$ ,  $C_0 \simeq (3.2 \pm 0.4) \times 10^{-4}$  for  $z_m = 1$  in these surveys, whereas  $C_0$  is predicted to be  $(5.1 \pm 0.8) \times 10^{-4}$  at  $1'$  in a model with unevolving power (i.e. with the power expected for  $\Lambda$ CDM at the present day as in section 2.1, but unchanged in the past),  $\sigma_{8,0} = 0.84 \pm 0.04$  and  $\Lambda$ CDM geometry ( $\Omega_m = 0.3, \Omega_{\text{tot}} = 1, H_0 = 72 \text{ km s}^{-1} \text{ Mpc}^{-1}$ ) calculated using equation (19).

However, we will see that there is considerable power in using the redshift information for each galaxy, as we will obtain significantly more accurate measurements of the evolution, and will be able to exclude no-growth models regardless of present-day power spectrum normalisation. We begin by making a direct detection of evolution with the 3-D shear field. We can do this by calculating the  $\chi^2$  fit of the no-evolution model to the data, and comparing with the  $\chi^2$  fit for, say, an evolving  $\Lambda$ CDM model ( $\Omega_m = 0.3, \Omega_{\text{tot}} = 1, H_0 = 72 \text{ km s}^{-1} \text{ Mpc}^{-1}$ ), in the first instance both with  $\sigma_{8,0} = 0.84$  (c.f. Spergel et al 2003). In the next section we will examine the effect of varying this normalisation and marginalising over cosmological parameters.

The sum we require for our  $\chi^2$  fit is given by

$$\chi^2 = \sum_{i,j} w_{ij} [(\gamma_{1,i} \gamma_{1,j} - C_1(\theta_{ij}, z_i, z_j))^2 + (\gamma_{2,i} \gamma_{2,j} - C_2(\theta_{ij}, z_i, z_j))^2], \quad (34)$$

where  $\gamma_1$  and  $\gamma_2$  are the two components of shear for a particular galaxy, in the frame where the  $x$ -axis is the line joining the two galaxies in question;  $w_{ij}$  are a set of weights which we will choose presently.  $i$  and  $j$  are indices for different galaxies, and  $C_1$  and  $C_2$  are the expected correlation functions between the two galaxies in the model, calculated using equations (21) and (22).

Here we choose a simple weighting  $w_{ij} = 1/\sigma_\gamma^4$ ,  $i \neq j$ , where  $\sigma_\gamma$  is the variance in one shear component. We choose this weighting as the error upon  $\gamma_{1,i} \gamma_{1,j}$  is entirely dominated by the random orientation of galaxies; therefore we have neglected off-diagonal elements of the covariance matrix of errors upon  $\gamma_{1,i} \gamma_{1,j}$ . In addition, we neglect the smoothing error associated with our redshift uncertainty of  $\Delta z \simeq 0.05$ ; assessment of the impact of this small smoothing term is left for future investigation. We are also invoking the Central Limit Theorem in order to use  $\chi^2$  to estimate uncertainties upon parameters, as any one product of galaxy shears does not have a Gaussian error.

In order to remove the impact of intrinsic alignments between galaxies, due to physical galaxy alignment instead of apparent alignment due to lensing, we reject galaxy pairs which are within  $\Delta z = 0.05$  of each other, if their comoving separation is less than  $1 \text{ Mpc}$ . We also remove, with the same prescription, near galaxy pairs in the background without redshift information, assigning to them the median redshift as described in Section 3.

The weighting equation (34) is  $1/\sigma_\gamma^4$  since, if our shear estimator  $\gamma_i$  is near Gaussian, we find that the probability distribution of  $\gamma_i \gamma_j$  (i.e. two independent Gaussian variables multiplied together) is given by

$$\text{Prob}(y = \gamma_i \gamma_j) = \frac{1}{\pi \sigma_\gamma^2} K_0 \left( \frac{y}{\sigma_\gamma^2} \right), \quad (35)$$

where  $K_0$  is a modified Bessel function of the second kind. This probability distribution,  $\text{Prob}(y)$ , has variance  $\sigma_\gamma^4$  as stated; this is found to be an excellent match to the variance of measured  $\gamma_i \gamma_j$  (both have value  $0.31^4$ ).

The no-evolution model we select is as described above, i.e.  $\Lambda$ CDM ( $\Omega_m = 0.3, \Omega_{\text{tot}} = 1, H_0 = 72 \text{ km s}^{-1} \text{ Mpc}^{-1}$ ) power at the present day with  $\sigma_{8,0} = 0.84$ ; however, this power remains constant at earlier epochs. An evolving  $\Lambda$ CDM geometry is assigned with parameters as above, evolving as appropriate to a given epoch; that is to say, the lack of evolution is directly in the power, not in the geometry. As described in Section 3, we apply the fit to two cases: in the first case, we include only galaxies with a reliable photometric redshift measurement. In the second case, we assign a redshift  $z = 0.95$  to objects without measured redshift, for both evolving and non-evolving measurements of  $\chi^2$ . (In the next section, we will include the effects of marginalisation over the allowed range of median redshift and Hubble parameter).

If we include the background objects with assigned median redshift, we find that the probability ratio between the no-evolution model and the  $\Lambda$ CDM model is  $\exp(\chi_{\text{noev}}^2 - \chi_{\Lambda\text{CDM}}^2)/2 = e^{-31.1}$ ; thus the no-evolution model is completely excluded given this simple two-model comparison. If one only uses objects with known redshifts, one finds a probability ratio of 49.4; i.e. the  $\Lambda$ CDM model is approximately 50 times more likely a model than the no-evolution model, given our data.

Thus we see that, using shear estimators together with photometric redshifts for each galaxy, we are immediately able to set powerful constraints on the evolution of structure. But we must now proceed to a fuller treatment for measuring the evolution, including the effect of power spectrum normalisation.

## 4.2 Measuring the evolution of the power spectrum

In this section, we seek to measure the slope of the mass power spectrum in the redshift direction, together with the present-day amplitude of the power spectrum. In order to achieve this, we use the parameterised power spectrum of equation (33), rescaled as  $P_\delta(k, w) = A k^\alpha e^{-sz}$ , and calculate from this the shear correlation functions as described in Section 2.2, using our standard  $\Lambda$ CDM geometry ( $\Omega_m = 0.3, \Omega_{\text{tot}} = 1, H_0 = 72 \pm 5 \text{ km s}^{-1} \text{ Mpc}^{-1}$  from Freedman et al 2001). We carry out the  $\chi^2$  calculation above (equation (34)), varying the parameters  $A$  (power spectrum amplitude at present day) and  $s$  (related to the gradient of the spectrum as a function of redshift), while fixing  $\alpha = -1.2$  as discussed in Section 2. We marginalise over  $H_0 = 72 \pm 5 \text{ km s}^{-1}$  and median redshift  $z \simeq 0.95 \pm 0.05$ .

The resulting constraints on the parameters  $A$  and  $s$  are shown in Figure 1. The panels show the constraints from the

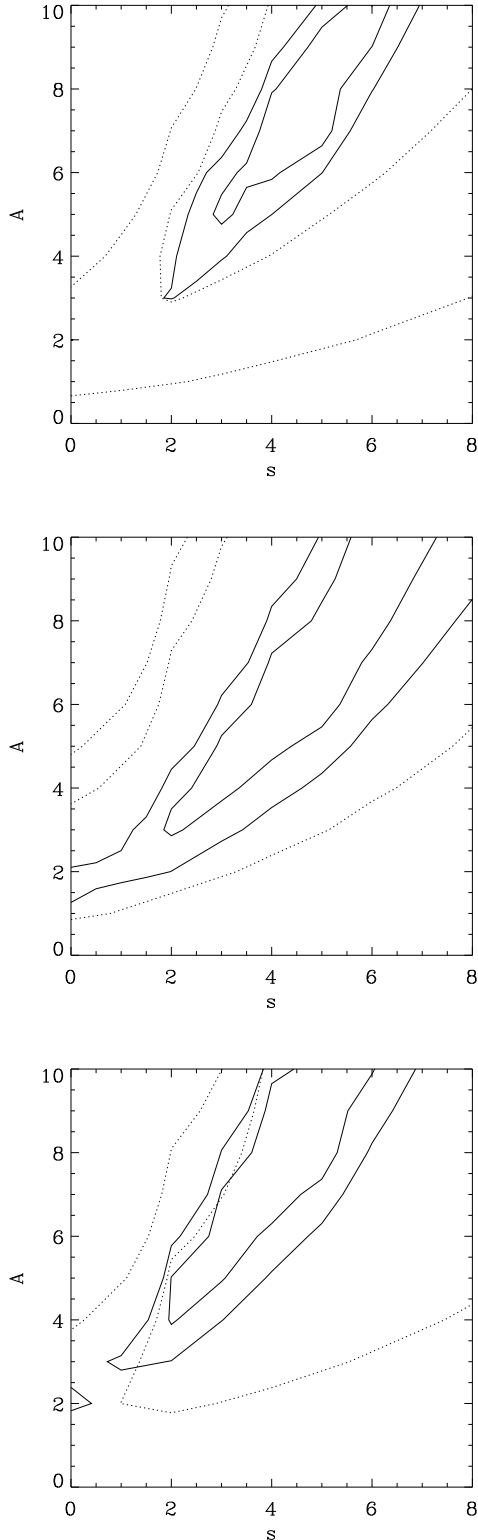


**Figure 1.** Joint constraints on power spectrum amplitude  $A$  and evolution slope  $s$  from COMBO-17 survey (CDFS and S11 fields). Top panel: combined constraints from the two fields. Dotted lines show the constraints from galaxies with known redshifts only. Contours display 1 and  $2\sigma$  confidence regions. Solid lines show constraints including galaxies with unknown redshift, assigned  $z=0.95$ . Middle panel: constraints from the CDFS field only. Bottom panel: constraints from the S11 field only.

combined fields, CDFS and S11 respectively; dotted lines show the constraints if we only include galaxies with known redshifts, while solid lines show constraints including the galaxies with unknown redshifts.

It is easy to understand the basic shape of the confidence contours; if one has a higher amplitude of power at the current epoch, one requires a more dramatic rate of growth to account for the shear estimates (c.f. the previous section, where we saw that a moderate present-day amplitude absolutely requires decreasing power as we increase redshift).

Note that our fit allows very large values of the present-day normalisation  $A$  and slope  $s$  (Figure 1 only shows the  $A - s$  region of interest; acceptable fit is achieved even for  $A = 100$ ). This is because the lensing predictions from a finite field are insensitive to the power and growth of power present at low redshift (c.f. discussion concerning Figure 2 below). Thus for our investigations, we will impose a prior  $A < 10$  corresponding to a rate of growth approximately three times faster than that expected for  $\Lambda$ CDM, as discussed below.

We find that  $s < 0$  is excluded at the  $1.9\sigma$  level if we include all galaxies, and at the  $1.2\sigma$  level if we only include galaxies with known redshifts. This initially appears to be a much lower level of confidence to that discussed in the previous section; however, here we are still allowing models which have very low present-day power spectrum amplitudes. If we require  $A > 3$ , corresponding to  $\sigma_8 \gtrsim 0.4$ , we find that  $s \leq 0$  is excluded at the  $7.7\sigma$  level if all galaxies are included, and at  $2.7\sigma$  in the known-redshift case; therefore we are again finding very strong rejection of the no-evolution model, if we require a reasonable present-day power spectrum amplitude.

Turning now to the actual measurements of  $A$  and  $s$  afforded by our fit, we find that our 2-D contours constrain  $s > 2(1\sigma)$  for CDFS or S11 independently (including galaxies with unknown redshifts). This is entirely consistent with our fiducial  $\Lambda$ CDM model, which is found to have (by fitting a tangent to the calculated power spectrum model) an initial ( $z = 0$ ) slope coefficient  $s = 1.7$  for  $k = 1\text{Mpc}^{-1}$  and  $s = 2.0$  for  $k = 50\text{Mpc}^{-1}$ .

The amplitudes of the two fields show significant variation from field to field, with best fit  $A = 3.2$  and  $A = 4.5$  at  $s = 2$  for CDFS and S11 respectively (including galaxies with unknown redshift); thus when the  $\chi^2$  are combined for the two fields, the reduced overlap artificially increases the acceptable values of  $s$  for the combined data. Clearly therefore, we will greatly benefit from applying the methodology to many more lines of sight.

A possible extension of this approach is to directly couch  $A$  in terms of  $\sigma_8$ ; however, since our phenomenological power spectrum model has a different  $k$  and  $z$  dependence to a full cosmologically parameterised power spectrum, values of  $\sigma_8$  calculated for our model do not have the conventional calibration. Instead, we will carry out the equivalent measurement of the normalisation of the power spectrum in terms of  $\sigma_8$  in section 4.3.

One should note the extraordinary improvement in accuracy arising from using our whole sample, as opposed to only those galaxies with known redshifts. The combined constraint upon  $A$  and  $s$  has improved by a factor of  $> 2$  for each field. This acts as a driving concern for future surveys; we would clearly wish to have a sample with known red-

shifts to  $R \simeq 25$ , which poses a serious challenge to current photometric redshift techniques.

We can use the information we have acquired on  $A$  and  $s$  to plot constraints upon the power spectrum growth itself. Since we can describe  $P_\delta = Ae^{-sz}k^\alpha$ , and since we have measured the probability distribution of  $A$  and  $s$ ,  $\text{Prob}(A, s)$ , we can calculate the probability of any particular value of  $P_\delta$  at a given  $z$ ,  $\text{Prob}(P_\delta)$ .

We calculate this by examining the cumulative probability distribution  $F$  for  $P_\delta$ , i.e. the probability that  $P_\delta$  is smaller than a certain value  $P_{\delta 0}$ . We see that

$$F = \int_0^{P_{\delta 0}} \text{Prob}(P_\delta) dP_\delta = \int_0^\infty dA \int_{\frac{1}{z} \log\left(\frac{A}{P_\delta}\right)}^\infty ds \text{Prob}(A, s). \quad (36)$$

Now  $\text{Prob}(P_\delta) = \partial F / \partial P_\delta$ , so

$$\text{Prob}(P_\delta) = \int_0^\infty \frac{dA}{P_\delta z} \text{Prob}\left(A, s = \frac{1}{z} \log\left(\frac{A}{P_\delta}\right)\right). \quad (37)$$

We can calculate this directly from our  $(A, s)$  probability contours. We plot the resulting constraints upon the power spectrum growth in Figure 2. Here, we have used the probabilities including the galaxies without known redshifts, as we found above that the constraints from the redshift sample are weak. Also plotted is the growth prediction for  $\Lambda$ CDM ( $\Omega_\Lambda = 0.7, \Omega_m = 0.3$ ) with  $\sigma_8 = 0.7$  (c.f. section 4.3); we see that the  $\Delta^2$  constraints are consistent (within  $2\sigma$ ) with this model, for  $0 < z < 1$ . Agreement is better between the model and an individual field, rather than the fields combined, as discussed above. Note that a  $k = 14 \text{Mpc}^{-1}$  has been chosen for this plot; the phenomenological model used presents us with an average,  $k$ -independent redshift evolution, as the model has  $k$  and  $z$  as independent variables.

The growth of the power spectrum shown on Figure 2 is skewed towards achieving high amplitude at the present day, with corresponding large  $s$ , simply because our small dataset cannot currently differentiate well between slow-growth low-amplitude and rapid-growth high-amplitude models. Since there is a large area in parameter space representing the latter, the overall constraints favour these while not excluding slower,  $\Lambda$ CDM growth. Larger surveys will be required in order to improve the measurement of matter power spectrum growth, by measuring the growth of the shear correlation function more accurately as a function of redshift and thus restricting the  $A - s$  degeneracy. With these larger surveys, the procedure we have outlined will allow detailed study of the collapse of structures in the Universe.

In this section, we have measured the growth rate and amplitude of the matter power spectrum using a phenomenological model. However, this is only one approach to the extraction of useful information from a 3-D shear field; instead of fitting a phenomenological model as above, we can directly fit the shear predictions for a range of cosmological parameters. We will carry out this analysis in the following section.

### 4.3 Constraints on the cosmological constant

Instead of a direct parameterisation of the slope of the power spectrum with redshift, we can characterise the 3-D shear data by the constraints which they provide on cosmological parameters. With the current small dataset, it is not

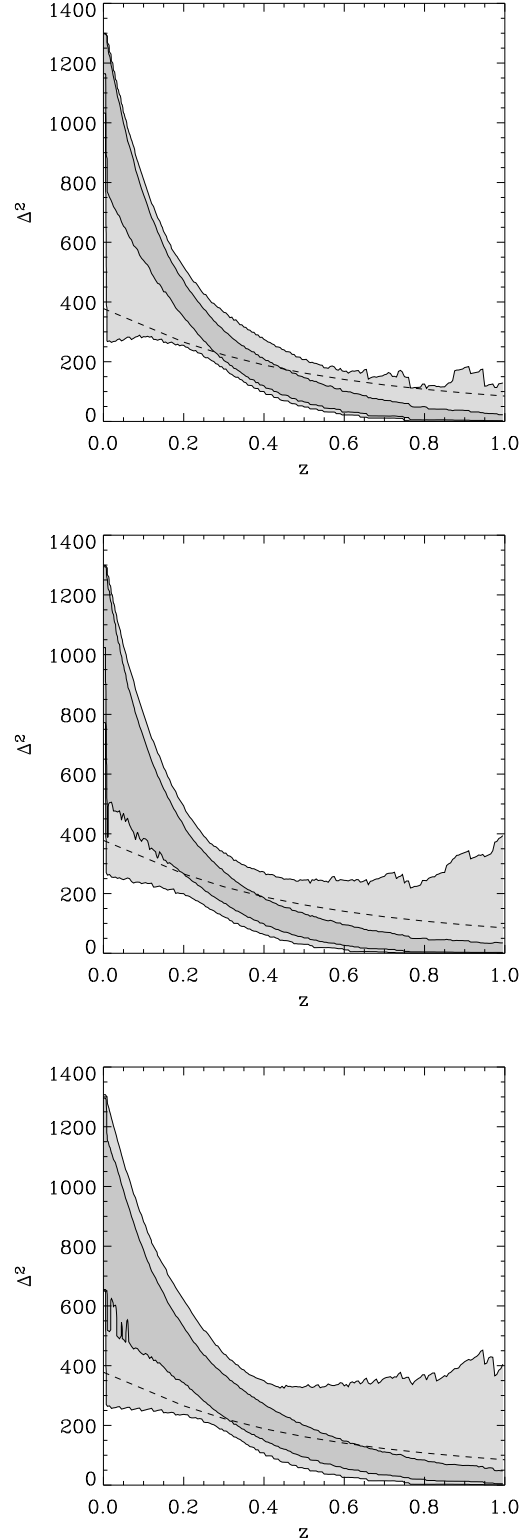


**Figure 2.** Constraints on power spectrum as a function of redshift  $z$ , displayed for  $k = 14 \text{Mpc}^{-1}$ . The contours show 1 and  $2\sigma$  confidence for the behaviour of the power spectrum at a given redshift. Also plotted (dashed line) is the prediction for  $\Lambda$ CDM with  $\sigma_8 = 0.7$ . Top panel: results for CDFS and S11 combined; middle panel: results for CDFS only; bottom panel: results for S11 only.



possible to obtain cosmologically interesting constraints on many parameters at once. Instead, here we will use priors from WMAP for most parameters, and examine the resulting constraints on the normalisation  $\sigma_8$  and cosmological constant  $\Lambda$  from the COMBO-17 data. Future work with large 3-D shear datasets will be able to obtain estimations of full parameter sets from shear alone.

#### 4.3.1 Non-flat Models

We choose in the first instance to use the Hubble Key Project and WMAP measurements of parameters  $H_0 = 72 \pm 5 \text{ km s}^{-1} \text{ Mpc}^{-1}$  and  $\Omega_b = 0.047 \pm 0.006$  (Freedman et al 2001, Spergel et al 2003), and examine the slice in parameter space at  $\Omega_m = 0.3$  allowing  $\Omega_\Lambda$  and  $\sigma_8$  to vary (i.e. we will allow non-flat models,  $\Omega_\Lambda + \Omega_m \neq 1$ ). This will enable us to examine the constraint from our 3-D lensing method on  $\Omega_\Lambda$  if  $\Omega_m$  is known. We calculate the 3-D shear correlation functions for this set of parameters as described in Section 2. We then make  $\chi^2$  fits to the data as above, varying  $\sigma_8$  in steps of 0.05 and  $\Omega_\Lambda$  in steps of 0.1.

The resulting weak constraints on these parameters, while either excluding or including the unknown redshift sample fixed at  $z = 0.95$  (with  $\pm 0.05$  marginalisation to account for the uncertainty in median redshift, plus marginalisation over  $H_0$ ), are shown in Figure 3. In the case where we use only galaxies with known redshift, we obtain only very broad constraints on  $\sigma_8$  and  $\Omega_\Lambda$ . We find an upper limit on  $\Omega_\Lambda$  of  $\Omega_\Lambda < 4.0 - 4.2\sigma_8$  at the  $1\sigma$  level, or  $\Omega_\Lambda < 5.15 - 4.8\sigma_8$  at the  $2\sigma$  level. These results also constrain  $\sigma_8$  to have a low normalisation,  $\sigma_8 < 0.70(0.93)$  at the  $1(2)\sigma$  confidence level for  $\Omega_\Lambda = 0.7$ . This is consistent with the  $\sigma_8$  normalisation found for the COMBO-17 dataset for a 2D cosmic shear analysis (Brown et al 2003). Perhaps this is not surprising for the two fields of interest here, as both are rather empty fields containing little evidence of substantial large-scale structure, other than the cluster in one chip of the S11 field. Therefore further fields will require analysis before one can obtain a definitive value for  $\sigma_8$  from this method.

If we include galaxies with unknown redshifts, assigned a redshift  $0.95 \pm 0.05$ , our constraints remain weak but show that the  $\Omega_\Lambda$  estimate does vary weakly with  $\sigma_8$ ; the best fit joint constraint line is  $\Omega_\Lambda = 5.6 - 7.7(\sigma_8 \pm 0.07)$ . This behaviour is as expected; the weakness of the dependence shows that  $\Lambda$ CDM and OCDM models have quite similar evolution over  $0 < z < 1$ . As seen above, these results give a low estimate of  $\sigma_8$  on our fields; note that we already expected these fields to give a low estimate for the spatial fluctuation of dark matter.

#### 4.3.2 Flat Models

An alternative means of deriving useful constraints from this small dataset is to fix  $\Omega_\Lambda + \Omega_m = 1$ , i.e. we can impose the flatness condition measured by WMAP ( $\Omega_{\text{tot}} = 1.02 \pm .02$  with Hubble key project  $H_0$  prior, Freedman et al 2001, Spergel et al 2003). With this condition, we can again make shear correlation function predictions, then obtain  $\chi^2$  fits to the data for various values of  $\sigma_8$  and  $\Omega_\Lambda$ , incrementing in units of 0.05 and 0.05 respectively. We marginalise over  $H_0$  and  $z_{\text{median}}$  as before.

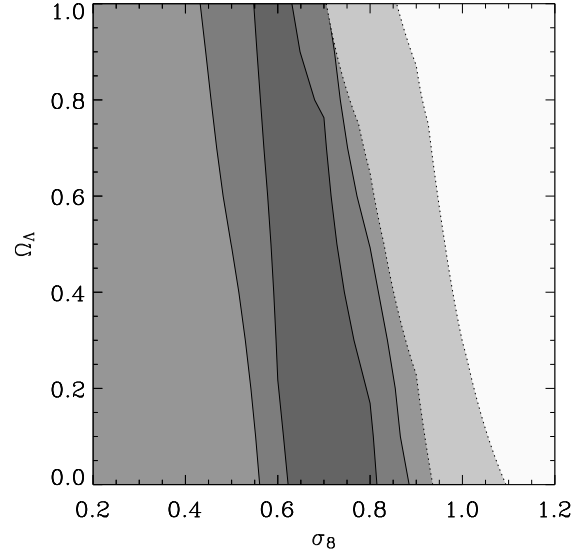


**Figure 3.** Constraints on  $\Omega_\Lambda$  and  $\sigma_8$  from the COMBO-17 survey, with  $\Omega_m$  fixed to be 0.3 and curvature allowed to vary arbitrarily. Dotted lines (and lightest two greyscales): constraints solely from sample with known redshifts. Solid lines (and darker two greyscales): constraints including galaxies with unknown redshift.

The results are shown in Figure 4, for the cases where we exclude and include the unknown redshift sample fixed at  $z = 0.95 \pm 0.05$ . Here we find that the constraints on  $\Omega_\Lambda$  or  $\Omega_m$  are substantially improved over the case where we do not prescribe flatness.

In the case where we exclude the unknown redshift galaxies, we find a weak constraint  $\Omega_\Lambda > 1 - 0.16\sigma_8^{-1.95}(1\sigma)$  or  $\Omega_\Lambda > 1 - 0.25\sigma_8^{-1.76}(2\sigma)$ . If we then force a prior  $\sigma_8 = 0.84 \pm 0.04$ , we obtain  $\Omega_\Lambda = 0.91^{+0.09}_{-0.27}$  at the  $2\sigma$  level, consistent with standard  $\Lambda$ CDM as defined above.

Again, these results offer a low normalisation of the matter power spectrum; for  $\Omega_\Lambda = 0.7$ , we require  $\sigma_8 < 0.72$  at the  $1\sigma$  level. As discussed in the previous section, this result is dominated by the fact that our two fields are devoid of significant large-scale structure; further fields will require measurement before cosmological implications can be conclusively drawn.

If we now include galaxies with unknown redshift, we find a best-fit constraint  $\Omega_\Lambda = 1 - 0.15(\sigma_8 \pm 0.04)^{-1.5}$ ,  $\sigma_8 < 0.72(1\sigma)$ . In the case where we impose a prior  $\sigma_8 = 0.84 \pm 0.04$ , we obtain  $\Omega_\Lambda = 0.83^{+0.06}_{-0.11}(2\sigma)$ . This, and the constraint directly from our contours  $\Omega_\Lambda < 0.76(1\sigma)$  is in accord with the concordance  $\Lambda$ CDM model; only the power spectrum normalisation is outside the range expected.

Despite the limitations due to the size of our dataset, these constraints are already impressive, and demonstrate the power of using 3-D information. Figure 4 compares the accuracies of the 2D analysis of Brown et al (2003, dashed lines) for only the CDFS and S11 fields with the current 3-D analysis (solid lines); clearly one gains very significantly from the inclusion of the redshift information, by a factor of  $> 2$  everywhere in uncertainty (beyond  $\sigma_8 > 0.4$ ). This holds out

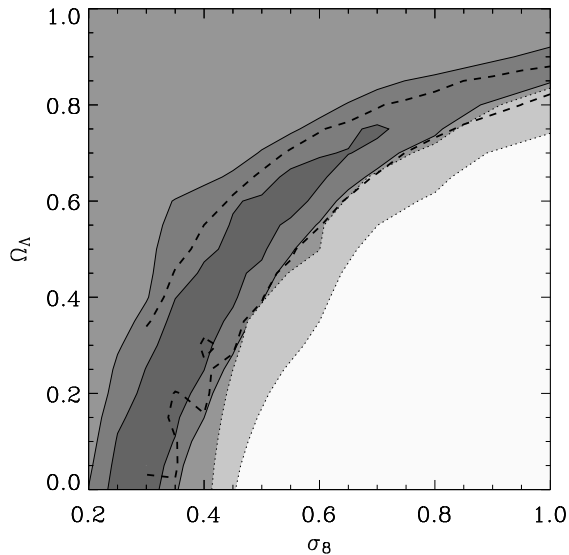


**Figure 4.** Constraints on  $\Omega_\Lambda$  and  $\sigma_8$ , with  $\Omega_\Lambda + \Omega_m$  fixed to be 1. Dotted line (and lighter two greyscales): constraints solely from sample with known redshifts. Solid line (and darker two greyscales): constraints including faint sample. Dashed lines show the constraints from our 2D lensing analysis in Brown et al (2003).

the promise of very precise measurements of cosmological parameters with future 3-D lensing surveys.

## 5 CONCLUSIONS

In this paper, we have explored the evolution of large-scale structure for redshifts  $z < 1$ . This has been achieved using weak gravitational lensing together with photometric redshifts for a set of galaxies, both measured upon two fields from the COMBO-17 survey (Wolf et al 2001).

We have described the construction of theoretical models of evolving matter power spectra, both in terms of phenomenology of the growth of structure, and in terms of characterisation of this growth with cosmological parameters. We have then shown how to calculate the shear power spectrum from this matter power spectrum, and vice versa. In particular, we have discussed the importance of the cross power spectrum for shears between redshift shells, and have related phenomenological models for evolution between the matter and shear cross power spectra.

In order to practically implement this theoretical framework, we have described the usefulness of the COMBO-17 survey for 3-D shear analysis, due to its accurate photometric redshifts for galaxies in the survey (with  $\Delta z \simeq 0.05$  for  $0 < z < 1.0$ ) and its well-studied shear catalogue.

We proceeded to apply a least squares estimator analysis to the data, finding that best-fit matter power spectra included significant evolution. In particular, we found that the growth rate expected for  $\Lambda$ CDM was approximately 50 times more likely than a zero evolution model, in the case where we ignore galaxies with unknown redshifts. However, we found that the best-fit rate of growth understandably depended sensitively upon the present-day amplitude of

the power spectrum. We calculated constraints upon  $\Delta^2(z)$ , finding a reasonable match with that predicted by  $\Lambda$ CDM for  $0 < z < 1$ , but allowing larger present-day amplitude of the power spectrum with more dramatic growth rates.

As an alternative route to extracting information from the 3-D shear field, we obtained least squares estimates of the cosmological constant and the normalisation of the power spectrum. We find low values of  $\sigma_8$  in this small area of sky, with best-fit constraints  $\Omega_\Lambda = 5.6 - 7.7(\sigma_8 \pm 0.07)$  and  $\Omega_\Lambda = 1 - 0.15(\sigma_8 \pm 0.04)^{-1.5}$ ,  $\sigma_8 < 0.72$  if we use WMAP priors on  $\Omega_m$  or  $\Omega_k$  respectively. We find that the latter constraint is a factor of 2 improvement upon the constraint obtained by 2D lensing for the same area of sky.

These results demonstrate that 3-D statistical lensing is a useful means of examining dark matter evolution. If one is interested in measuring only cosmological parameters, this method is a complementary alternative to measuring 2-D higher-order statistics of the shear field; the question of the comparative (and combined) merits of the two approaches is the subject of ongoing research (c.f. Benabed & van Waerbeke 2003, Refregier et al 2003). However, if one seeks a direct measurement of the dark matter evolution itself, 3-D methods such as the one explored here are essential. With large multi-colour imaging surveys in the next few years such as that of SNAP (Rhodes et al 2004), the potential of this approach will be fully realised, affording measurements of the cosmological constant and dark energy equation of state parameters to unprecedented accuracy, together with precise reconstructions of the growth of the power spectrum as a function of redshift.

## ACKNOWLEDGMENTS

DJB, MG and MLB are supported by a PPARC Postdoctoral Fellowship; ANT is supported by a PPARC Advanced Fellowship. CW was supported by the PPARC Rolling Grant in Observational Cosmology at the University of Oxford. We thank Alan Heavens and Hans-Walter Rix for extremely useful discussions.

## REFERENCES

- Bacon D., Massey R., Refregier A., Ellis R.S., 2003, MNRAS, 344, 673.
- Bacon D. J., Taylor A. N., 2003, MNRAS, 344, 1307.
- Bardeen J. M., Bond J. R., Kaiser N., Szalay A. S., 1986, ApJ, 304, 15.
- Bartelmann M., Schneider P., 2001, Phys. Rep., 340, 291.
- Blandford R. D., Saust A. B., Brainerd T. G., Villumsen J. V., 1991, MNRAS, 251, 600.
- Benabed K., van Waerbeke L., 2003, submitted to PhysRevD, astro-ph/0306033.
- Bernstein G., Jain B., 2004, ApJ, 600, 17.
- Bond J. R., Efstathiou G., 1984, ApJ, 285, 45.
- Brown M. L., Taylor A. N., Bacon D. J., Gray M. E., Dye S., Meisenheimer K., Wolf C., 2003, MNRAS, 341, 100.
- Carroll S. M., Press W. H., Turner E. L., 1992, ARA&A, 30, 499.
- Efstathiou G., Bond J. R., White S. D. M., 1992, MNRAS, 258, 1.
- Freedman W. L., Madore B. F., Gibson B. K., Ferrarese L., Kelson D. D., Sakai S., Mould J. R., Kennicutt R. C., Ford H. C.,

- Graham J. A., Huchra J. P., Hughes S. M. G., Illingworth G. D., Macri L. M., Stetson P. B., 2001, *ApJ*, 553, 47.
- Gray M. E., Taylor A. N., Meisenheimer K., Dye S., Wolf C., Thommes E., 2002, *ApJ*, 568, 141.
- Heavens A., 2003, *MNRAS*, 343, 1327.
- Heymans C., Heavens A., 2003, *MNRAS*, 339, 711.
- Heymans C., Brown M., Heavens A., Meisenheimer K., Taylor A., Wolf C., 2004, *MNRAS*, 347, 895.
- Hoekstra H., Yee H., Gladders M., Barrientos L. F., Hall P., Infante L., 2002, *ApJ*, 575, 55.
- Hu W., 1999, *ApJL*, 522, 21.
- Hu W., Keeton C. R., 2002, submitted to *PRD*, astro-ph/0205412.
- Hu W., 2002, *PhysRevD*, 66, 083515.
- Huterer D., 2002, *PhysRevD*, 65.
- Jain B., Taylor A., 2003, *PhysRevLett*, 91, 141302.
- Jarvis M., Bernstein G. M., Fischer P., Smith D., Jain B., Tyson J. A., Wittman D., 2003, *AJ*, 125, 1014.
- Kaiser N., Squires G., Broadhurst T., 1995, *ApJ*, 449, 460.
- King L., Schneider P., 2002a, *A&A*, 396, 411.
- King L., Schneider P., 2002b, *A&A*, 398, 23.
- Ma C.-P., Fry J. N., 2000, *ApJ*, 543, 503.
- Peacock J. A., Smith R. E., 2000, *MNRAS*, 318, 1144.
- Pen U.-L., Lu T., van Waerbeke L., Mellier Y., 2003, *MNRAS*, 346, 994.
- Percival W. J., Sutherland W., Peacock J. A., Baugh C. M., Bland-Hawthorn J., Bridges T., Cannon R., Cole S., Colless M., Collins C. et al, 2002, *MNRAS*, 337, 1068.
- Phleps S., Meisenheimer K., 2003, *A&A*, 407, 855.
- Refregier R., Massey R., Rhodes J., Ellis R., Albert J., Bacon D., Bernstein G., McKay T., Perlmutter T., 2003, submitted to *ApJ*, astro-ph/0304419.
- Refregier R., 2003, *ARA&A*, 41, 645.
- Rhodes J., Refregier A., Massey R., Albert J., Bacon D., Bernstein G., Ellis R., Jain B., Kim A., Lampton M. et al, 2004, *APh*, 20, 377.
- Seljak U., 1998, *ApJ*, 506, 64.
- Seljak U., 2000, *MNRAS*, 318, 203.
- Smith R. E., Peacock J. A., Jenkins A., White S. D. M., Frenk C. S., Pearce F. R., Thomas P. A., Efstathiou G., Couchman H. M. P., 2003, *MNRAS*, 341, 1311.
- Spergel D. N., Verde L., Peiris H. V., Komatsu E., Nolte M. R., Bennett C. L., Halpern M., Hinshaw G., Jarosik N., Kogut A., Limon M., Meyer S. S., Page L., Tucker G. S., Weiland J. L., Wollack E., Wright E. L., 2003, *ApJS*, 148, 175.
- Sugiyama N., 1995, *ApJS*, 100, 281.
- Taylor A. N., 2001, submitted to *Phys Rev Lett*, astro-ph/0111605.
- Taylor A. N., Bacon D. J., Gray M. E., Wolf C., Meisenheimer K., Dye S., Borch A., Kleinheinrich M., Kovacs Z., Wisotzki L., 2004, submitted to *MNRAS*.
- Van Waerbeke L., Mellier Y., Radovich M., Bertin E., Dantel-Fort M., McCracken H. J., Le Fevre O., Foucaud S., Cuillandre J.-C., Erben T., Jain B., Schneider P., Bernardeau F., Fort B., 2001, *A&A*, 374, 757.
- Van Waerbeke L., Mellier Y., astro-ph/0305089.
- Wittman D., Tyson J. A., Margoniner V. E., Cohen J. G., Dell'Antonio I. P., 2001, *ApJ*, 557, 89.
- Wittman D., Margoniner V. E., Tyson J. A., Cohen J. G., Becker A. C., Dell'Antonio I. P., 2003, *ApJ*, 597, 218.
- Wolf C., Meisenheimer K. & Roeser H.-J., 2001, *A&A*, 365, 660.